Influence of Dy³⁺ Ions on the Optical Characteristics of Nanoscaled $Y_{1-x}Dy_xVO_4$ Phosphors

Hao-Ying Lu* and Meng-Han Tsai

The Department of Electronic Engineering, National Quemoy University, Kinmen 89250, Taiwan

Nanoscaled $Y_{1-x}Dy_xVO_4$ phosphors can be obtained via the modified chemical coprecipitation method. With the precipitant and centrifugation, the phosphors can be quickly synthesized within 2.5 h. From the X-ray diffraction (XRD) patterns, the phosphor with a 1000 °C thermal treatment possesses optimal crystallinity. All YVO_4:Dy³⁺ phosphors exhibiting a tetragonal structure can emit two light bands. One is located at 484 nm and the other at 576 nm. These two emission peaks appear as a result of the following electron transitions, $^4F_{9/2} \rightarrow {}^6H_{15/2}$ and $^4F_{9/2} \rightarrow {}^6H_{13/2}$. From the relation between the photoluminescence (PL) intensities and Dy³⁺ concentrations, the $Y_{1-x}Dy_xVO_4$ phosphor with 0.8% Dy³⁺ ions possesses the optimal emission. When the concentration of Dy³⁺ ions increases to 1.0%, the concentration quenching effect is observed. According to the Commission Internationale de L'Eclairage (CIE) diagram, the color coordinates of $Y_{0.992}Dy_{0.008}VO_4$ phosphor are located within the white-light area.

1. Introduction

During the past decades, people have suffered from abrupt climate changes, such as global warming, frequent cold and heat waves, frequent typhoons, the melting of glaciers and the rising of sea levels. These dramatic changes still influence the earth and human beings. Based on modern research, scientists believe that all climate changes originate from human activities, especially from the constant demand for energy. After the Fukushima nuclear accident, people were eager to obtain electricity from fossil-fuel power stations instead of nuclear power plants. However, burning fossil fuel leads to increases in carbon dioxide emission, which results in the greenhouse effect. In accordance with these reasons, the development of energy-saving technology has become a significant goal. In daily life, lighting consumes 19.3% of total power consumed. If people used light-emitting diodes (LEDs) to replace fluorescent lamps, the power consumed by lighting can be significantly reduced. This makes LEDs the potential lighting devices for this century.

In our research, the YVO_4-based phosphors chosen as emitting materials can be used as the emitting layer in LEDs or can be coated onto ultraviolet LEDs to emit white light. Due to their excellent stability with respect to chemicals and temperature, YVO_4 phosphors are considered to be promising materials for application to optical devices.[1] Among YVO_4-based phosphors, the red-light YVO_4:Eu³⁺ phosphors have been extensively used in televisions, cathode ray tubes (CRTs), field emission displays (FEDs), and plasma display panels (PDPs).[2–4] Because of the 4f–4f and

---

*Corresponding author: e-mail: hylu@nqu.edu.tw

5d–4f transitions, the rare-earth elements (REEs) chosen as the active centers to emit different colors of light have attracted the interest of many scientists who have investigated and synthesized REEs-based phosphors.[5] In 1975, Sommerdijk and Bril reported that the Dy^{3+} active center can simultaneously emit two bands located at 470–500 and 570–600 nm.[6] Then, Cavalli *et al*. further indicated that these two emission bands result from the $^4F_{9/2} \rightarrow {}^6H_{15/2}$ and $^4F_{9/2} \rightarrow {}^6H_{13/2}$ transitions.[7] In 2007, Su *et al*. suggested that the intensity ratio of blue and yellow emission bands could be modified to obtain white-light phosphors.[8]

Based on these advantages, different synthetic methods were applied to produce YVO_4-based phosphors in recent years. Zhou and Lin used two-step spray pyrolysis to synthesize a $YVO_4{:}Dy^{3+}$ phosphor. This method takes 10 h to complete the whole synthesis, and the average size of the resultant particle is larger than 1 μm.[9] In 2008, Chen *et al*. produced a YVO_4 phosphor via hydrothermal synthesis.[10] The entire process requires 28 h to produce nanorods. In addition, the sol–gel method was adopted to synthesize the $YP_xV_{1-x}O_4$ phosphor. After 30 h, phosphors with average particle size of 30 to 70 nm could be obtained.[11] Some research teams used solid state methods to obtain YVO_4-based phosphors. Under high-temperature treatment for 12 h, phosphors with a particle size around 0.5 μm could be synthesized.[12,13] Additionally, the chemical coprecipitation method is a common method to synthesize YVO_4 phosphor; it usually takes several days to complete the entire process.[14–16] In this study, the modified chemical coprecipitation method was adopted to enable the synthesis. With suitable thermal treatments, phosphors with an average size around 50 to 100 nm can be obtained within 2.5 h.

2.   Materials and Methods

2.1   Materials

In this study, yttrium nitrate hexahydrate $Y(NO_3)_3 \cdot 6H_2O$ (99.9%, Alfa Aesar), dysprosium nitrate pentahydrate $Dy(NO_3)_3 \cdot 5H_2O$ (99.9%, Alfa Aesar), and ammonium vanadate NH_4VO_3 (99.5%, Acros Organics) were used as the starting materials.

2.2   Synthesis of $Y_{1-x}Dy_xVO_4$ nanophosphors

At first, $Y(NO_3)_3 \cdot 6H_2O$, $Dy(NO_3)_3 \cdot 5H_2O$, and NH_4VO_3 were dissolved in distilled water at the stoichiometric ratio and the solution was stirred for 30 min at room temperature. Second, a 1% ammonia solution was used as the precipitant and added into the solution. With the addition of ammonia, the pH value of the solution was adjusted to 9.0, and the solution was placed for 30 min. Then, a white precipitate could be observed and separated directly by centrifugation. Third, the precipitate was washed with distilled water and ethanol several times. Finally, the dried precipitate was used as the precursor to synthesize the $Y_{1-x}Dy_xVO_4$ phosphors by suitable thermal treatment in air atmosphere for 1 h.

2.3   Alkaline-washing process

The precipitate obtained was washed with ammonia and dried directly. Then, the dried powders were used as the precursor for processing with further thermal treatments.

2.4   Characterization

The crystal structures of the phosphors were characterized using a Rigaku Miniflex II desktop X-ray diffractometer with CuKα radiation (θ, 10 to 40°; step, 0.01°). The size of the particles and morphologies of the phosphors were investigated using a field-emission scanning electron microscope (FE-SEM, JEOL JSM-6500F) with 15 kV accelerating voltage. The photoluminescence (PL) spectra and the PL excitation (PLE) spectra were recorded using a fluorescence spectrophotometer (Hitachi F-2700). All measurements were carried out at room temperature.

3.   Results and Discussion

Figure 1 shows the X-ray diffraction (XRD) patterns of YVO_4 nanopowders prepared at various treatment temperatures. As can be seen from this figure, the synthesized powders exhibited a tetragonal crystal structure (JCPDS 11-0254) and possessed a $ZrSiO_4$-type structure with dipyramidal symmetry. When the temperature of the thermal treatment was increased to 1200 °C, another phase appeared. Comparing this result with the JCPDS 44-0390 pattern, these peaks located at 28.9 and 29.3° belong to $Y_8V_2O_{17}$. As the temperature of the thermal treatment was increased from 600 to 1200 °C, the intensity of peak (2 0 0) increased. Compared with all the XRD patterns, the relative intensity ratio [for samples 1–3, Eq. (1); for sample 4, Eq. (2)] increased from 0.22 to 0.29 (see Table 1).
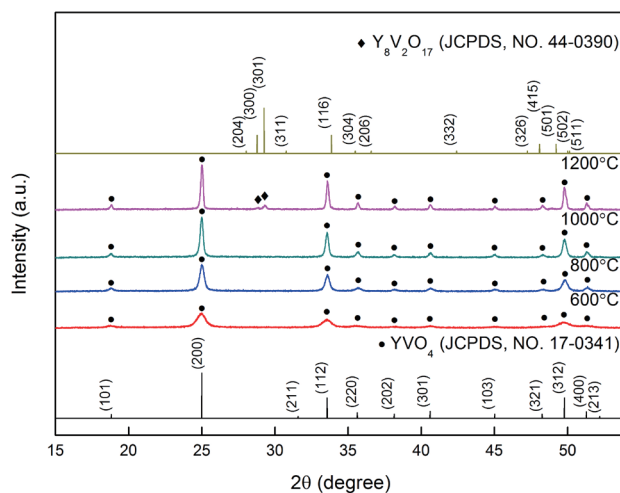

Fig. 1.   (Color online) XRD patterns of YVO_4 powders prepared at different thermal treatment temperatures.

Table 1
FWHM and relative intensity ratio of YVO_4 powders prepared at different treatment temperatures.

	Sample 1 600 °C	Sample 2 800 °C	Sample 3 1000 °C	Sample 4 1200 °C
FWHM	0.76°	0.39°	0.26°	0.20°
Relative intensity ratio	0.22	0.27	0.29	0.27

$$I_{200}/(I_{101} + I_{200} + I_{211} + I_{112} + I_{220} + I_{202} + I_{301} + I_{103} + I_{321} + I_{312} + I_{400}) \tag{1}$$

$$I_{200}/(I_{101} + I_{200} + I_{211} + I_{112} + I_{220} + I_{202} + I_{301} + I_{103} + I_{321} + I_{312} + I_{400} + I_{300} + I_{301}) \tag{2}$$

This means that the atoms have more kinetic energy when they crystallize at higher temperature, which results in a larger value of the relative intensity ratio. However, when the temperature of treatment was increased to 1200 °C, the relative intensity ratio was reduced to 0.27. Referring to Fig. 1, this suggests that YVO_4 uses thermal energy to change the structure, and hence the XRD peaks of $Y_8V_2O_{17}$ appear. In addition, the full-width half-maximum (FWHM) value of peak (2 0 0) decreases with treatment temperature (see Table 1). According to the Scherrer formula, the size of particles increases with the treatment temperature. Table 2 shows the lattice constants of YVO_4 phosphors prepared at different thermal treatment temperatures. From this table, the lattice constants in 3 axes approached those of JCPDS 11-0254 as the temperature was increased. To prevent the formation of $Y_8V_2O_{17}$ and obtain better crystallinity, 1000 °C was chosen as the optimal treatment temperature.

The XRD patterns of $Y_{1-x}Dy_xVO_4$ phosphors thermally treated at 1000 °C are shown in Fig. 2. In this figure, no structural differences can be observed with increasing Dy^{3+} concentration. All phosphor samples still exhibit the tetragonal structure. Table 3 shows the relation between the lattice constants and the concentration of active centers. From this table, no regular trend in lattice constants can be discerned in any axis. All lattice constants of phosphors are close to the ones of YVO_4. Two assumptions are used to explain this phenomenon. First, the radii of Y^{3+} and Dy^{3+} ions are 0.900 and 0.912 Å, respectively. Because the difference in radius between Y^{3+} and Dy^{3+}

Table 2
Lattice constants of YVO_4 phosphors prepared at different thermal treatment temperatures.

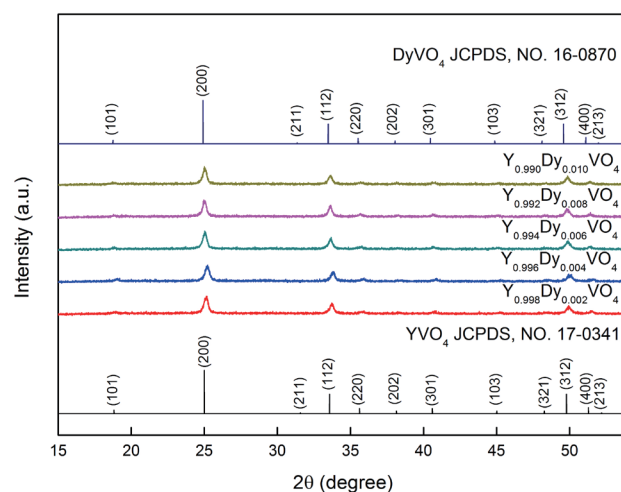| Lattice constant	JCPDS YVO$_4$	Treatment temperature			
		600 °C	800 °C	1000 °C	1200 °C
a	7.119 Å	7.088 Å	7.089 Å	7.108 Å	7.111 Å
b	7.119 Å	7.088 Å	7.089 Å	7.108 Å	7.111 Å
c	6.289 Å	6.271 Å	6.272 Å	6.286 Å	6.287 Å

Fig. 2. (Color online) XRD patterns of $Y_{1-x}Dy_xVO_4$ phosphors with different dopant concentrations. All samples were treated at 1000 °C.

ions is very small, this difference cannot influence the lattice constants very much. Second, the light dopant concentration (the maximum is 1%) also cannot influence the lattice constant much as well, especially because the radii of Y^{3+} and Dy^{3+} ions are so similar. These two factors result in the similar lattice constants shown in Table 3.

Figure 3 shows the PLE spectra of $Y_{1-x}Dy_xVO_4$ phosphors. In this figure, all PLE curves trend upward toward the left area. Referring to other reports, a broad and strong absorption band should exist in that area, but because of the detection limit of the instrument (Hitachi F-2700), the spectra between 250 and 345 nm are ignored. According to the report of Zhou and Lin, a broad and strong absorption band is located at 308 nm.[9] This strong band is due to the absorption of VO_4^{3-} groups. The stimulated charges transfer from O^{2-} ligands to V^{5+} atoms, and then the energy absorbed by VO_4^{3-} groups transfers into the Dy^{3+} atoms. This mechanism results in the strong absorption band between 250 and 345 nm in the PLE spectra. In addition to the strong absorption band, three narrow absorption peaks originating from the f-f transitions within Dy^{3+} $4f^9$ configuration are observed in Fig. 3.[3] These three peaks located at 352, 366, and 390 nm are the result of the following electron transitions: $^6H_{13/2} \rightarrow {}^4M_{15/2} + {}^6H_{7/2}$, $^6H_{13/2} \rightarrow {}^4I_{11/2}$, and $^6H_{13/2} \rightarrow {}^4M_{19/2}$, respectively.[11,16] The absorption peak located at 352 nm is the strongest one of these three and is chosen as the excitation wavelength for the following PL measurements. Between these five samples, the YVO_4 phosphor with 0.8% Dy^{3+} reveals the strongest absorption.

In Fig. 4, the PL spectra of $Y_{1-x}Dy_xVO_4$ phosphors are shown. Two emission peaks located at 484 and 576 nm are observed. These two emission peaks appear as a result of the following

Table 3
Lattice constants of $Y_{1-x}Dy_xVO_4$ phosphors with different active center concentrations. Dy^{3+} concentration starts at 0.2% and increases to 1%.

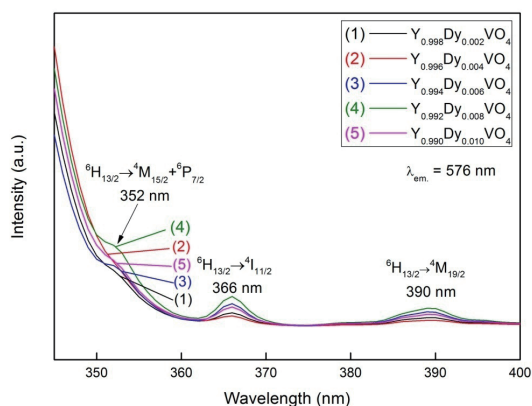| Lattice constant	$Y_{1-x}Dy_xVO_4$ phosphors, x = 0.002 to 0.010				
	0.002	0.004	0.006	0.008	0.010
a	7.100 Å	7.095 Å	7.114 Å	7.111 Å	7.112 Å
b	7.100 Å	7.095 Å	7.114 Å	7.111 Å	7.112 Å
c	6.277 Å	6.275 Å	6.284 Å	6.290 Å	6.279 Å

Fig. 3. (Color online) PLE spectra of YVO_4:Dy^{3+} phosphors with different active center concentrations; the emission wavelength is 576 nm.
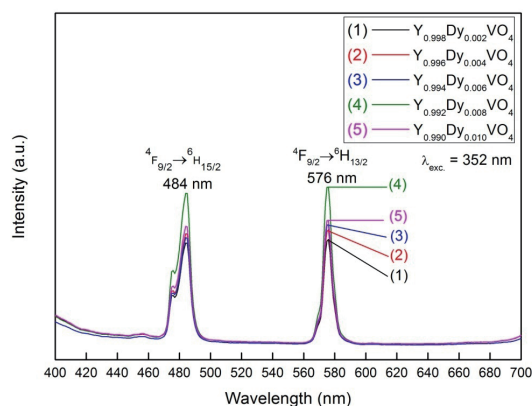

Fig. 4. (Color online) PL spectra of YVO_4:Dy^{3+} phosphors with different active center concentrations; the excitation wavelength is 352 nm.

electron transitions: $^4F_{9/2} \rightarrow {}^6H_{15/2}$ and $^4F_{9/2} \rightarrow {}^6H_{13/2}$. The emission peak located at 484 nm is a blue-light band, and another located at 576 nm is a yellow-light band. When these two emission bands were combined together, the chromaticity changes and locates within the white-light area. Figure 5 shows the Commission Internationale de L'Eclairage (CIE) chromaticity diagram of the $Y_{0.992}Dy_{0.008}VO_4$ phosphor. The color coordinates locate within the white-light area, but the chromaticity is near the yellow area. If the intensity ratio of the blue to the yellow bands can be adjusted, the chromaticity could be pure white light.

Figure 6 shows the relation between the concentration of active centers and emission intensities. From this figure, the emission intensity of $Y_{1-x}Dy_xVO_4$ phosphor increased with the early increase in Dy^{3+} concentration. As the Dy^{3+} concentration increased to 0.8%, the $Y_{0.992}Dy_{0.008}VO_4$ phosphor produced the strongest PL intensity. When the Dy^{3+} concentration increased from 0.8 to 1%, the PL intensity of the $Y_{1-x}Dy_xVO_4$ phosphor decreased. The concentration quenching effect can explain this phenomenon. When the Dy^{3+} concentration is above 0.8%, the mean distance between Dy^{3+} ions becomes smaller. When a Dy^{3+} ion releases energy by radiation, another Dy^{3+} ion might absorb the energy due to the small distance between Dy^{3+} ions and release the energy again as phonons. This energy release path causes the PL intensity to decrease. Additionally, the intensity ratio of the blue to the yellow bands (I_B/I_Y) is similar for different Dy^{3+} concentrations. This observation means that the chromaticity of all the phosphors is similar.

Figure 7 shows images of the surface morphology of the YVO_4-based powders. Four samples are shown in the figure. The first two samples (a and b) did not have the alkaline-washing process, while the other two (c and d) were given the alkaline-washing process. First, the sample was well-dispersed in deionized water by an ultrasonicator. Second, the upper part of the solution was dropped onto a carbon conductive tape, and then the tape was dried at 90 °C. These steps were repeated 10 times to complete the preparation of the SEM samples. From Figs. 7(a) and 7(b), the diameter of spherical phosphor was between 60 and 94 nm. Compared with Figs. 7(c) and 7(d), the diameter of the samples treated with the alkaline-washing process was reduced to 50
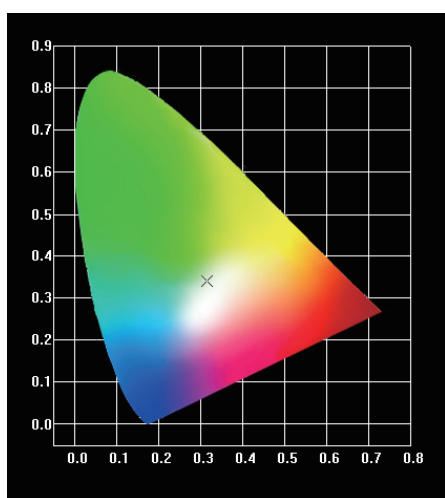

Fig. 5. (Color online) CIE chromaticity diagram of $Y_{0.992}Dy_{0.008}VO_4$ phosphor.
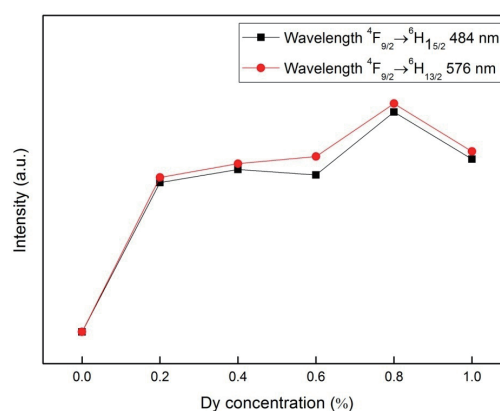

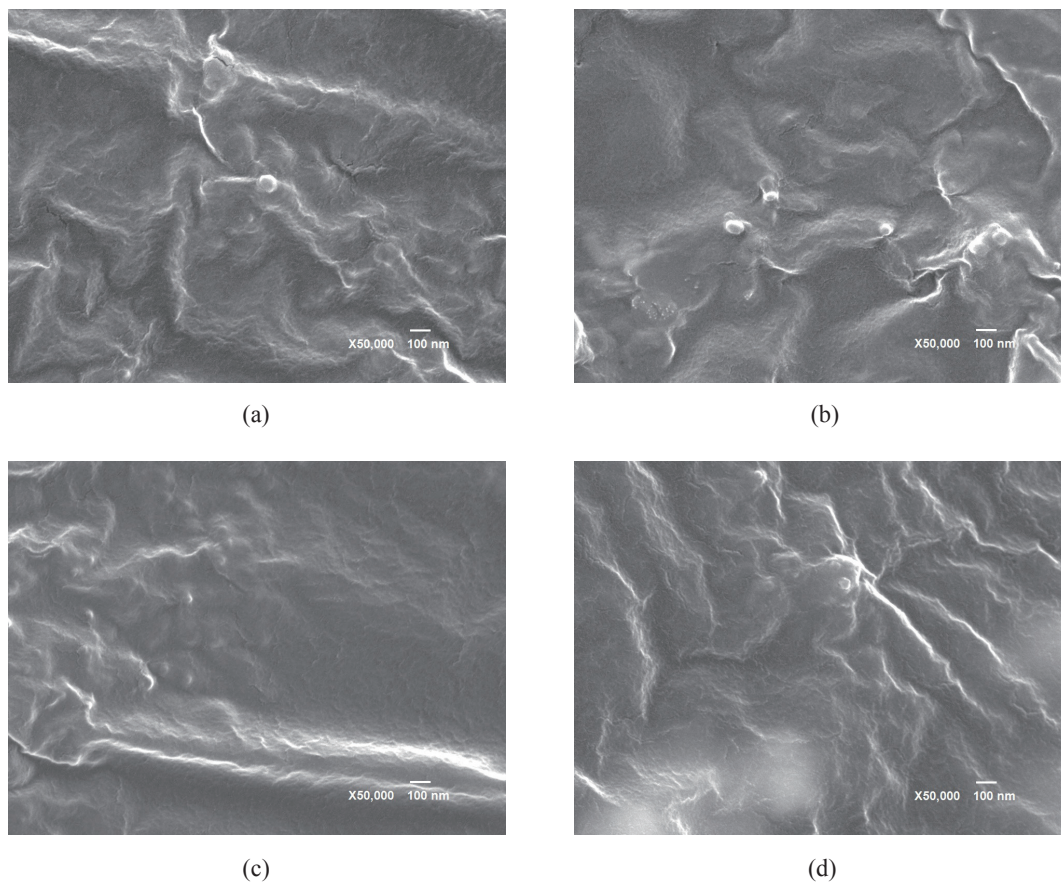Fig. 6. (Color online) Peak intensities of YVO_4:Dy^{3+} phosphors with different active center concentrations.

Fig. 7.   SEM images of (a) YVO_4, (b) $Y_{0.992}Dy_{0.008}VO_4$, (c) YVO_4 with the alkaline-washing process, and (d) $Y_{0.992}Dy_{0.008}VO_4$ with the alkaline-washing process.
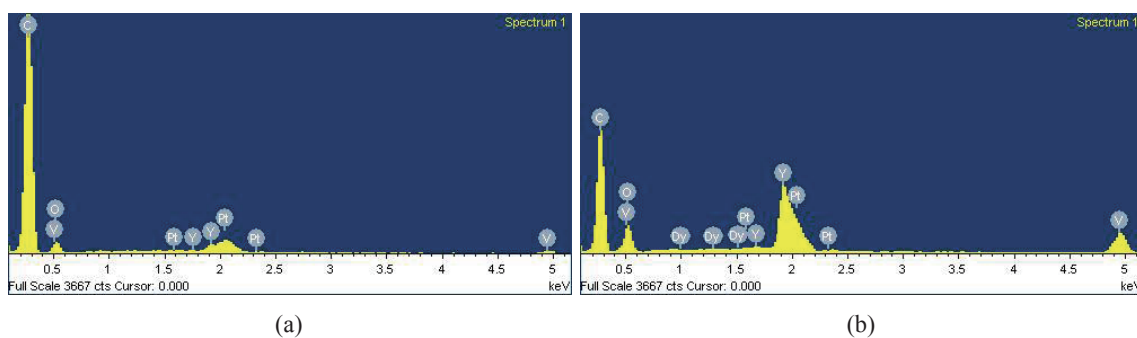

Fig. 8.   (Color online) EDS profiles of (a) YVO_4 and (b) $Y_{0.992}Dy_{0.008}VO_4$ phosphors.

nm. It is believed that the alkaline-washing process effectively reduces the size of the particles. Additionally, energy-dispersive X-ray spectroscopy (EDS) profiles are shown in Fig. 8. From this figure, the signals due to carbon and platinum originate from the carbon conductive tape and the sputtered metal, respectively. No signals of other elements were observed in these samples, and all compositions were consistent with those of the starting materials.

4.   Conclusions

Nanoscaled $Y_{1-x}Dy_xVO_4$ phosphors can be synthesized quickly via the modified chemical coprecipitation method. After a 1000 °C thermal treatment for 1 h, the diameter of the sphere-shaped particles was approximately 60 to 94 nm. The alkaline-washing process was applied to reduce the particle size. In our work, the diameter of the particles treated with the alkaline-washing process was about 50 nm. In the PL spectra, two emission peaks were observed. One was a blue-light band and the other a yellow-light band. These two emission peaks resulted in the white-light emission. From the CIE diagram, the color coordinates were located at (0.314, 0.341). Additionally, the concentration quenching effect was also observed from the relation between the PL intensities and the Dy^{3+} concentrations. The YVO_4 phosphor with 0.8% Dy^{3+} possessed the strongest emission in this study. Through the modified chemical coprecipatation method and suitable thermal treatments, nanoscaled $YVO_4:Dy^{3+}$ phosphors can be obtained within 2.5 h. It is believed that this is an effective method to obtain the nanoscaled phosphors. These phosphors may be considered for the emitting materials in LEDs or may be coated onto ultraviolet LEDs to enable the emission of white light.

References

 1   H. W. Zhang, X. Y. Fu, S. Y. Niu, G. Q. Sun, and Q. Xin: Mater. Lett. **61** (2007) 308.
 2   A. K. Levine and F. C. Palilla: Appl. Phys. Lett. **5** (1964) 118.
 3   M. Yu, J. Lin, Z. Wang, J. Fu, S. Wang, H. J. Zhang, and Y. C. Han: Chem. Mater. **14** (2001) 2224.
 4   F. He, P. P. Yang, N. Niu, W. Wang, S. Gai, D. Wang, and J. Lin: J. Colloid Interface Sci. **343** (2010) 71.
 5   L. Chen, G. Liu, Y. Liu, and K. Huang: J. Mater. Process. Technol. **198** (2008) 129.
 6   J. L. Sommerdijk and A. Bril: J. Electrochem. Soc. **122** (1975) 952.
 7   E. Cavalli, M. Bettinelli, A. Belletti, and A. Speghini: J. Alloys Compd. **341** (2002) 107.
 8   Q. Su, H. Liang, C. Li, H. He, Y. Lu, J. Li, and Y. Tao: J. Lumin. **122** (2007) 927.
 9   Y. H. Zhou and J. Lin: J. Alloys Compd. **408** (2006) 856.
10   L. Chen, G. Liu, Y. Liu, and K. Huang: J. Mater. Process. Technol. **198** (2008) 129.
11   A. Bao, H. Yang, C. Tao, Y. Zhang, and L. Han: J. Lumin. **128** (2008) 60.
12   Z. P. Ci, Y. H. Wang, and J. C Zhang: Chin. Phys. B **19** (2010) 057803.
13   F. Angiuli, F. Mezzadri, and E. Cavalli: J. Solid State Chem. **184** (2011) 1843.
14   C. V. Devi, G. Phaomei, N. Yaiphaba, and N.R. Singh: J. Alloys Compd. **583** (2014) 259.
15   X. Q. Su and B. Yan: J. Non-Cryst. Solids **351** (2005) 3542.
16   Y. Y. He, M. Q. Zhao, Y. Y. Song, and G. Y. Zhao: Mater. Res. Bull. **47** (2012) 1821.